OPEN ACCESS
IOP Publishing

Letters
Journal of Physics D: Applied Physics

J. Phys. D: Appl. Phys. **50** (2017) 18LT01 (9pp)
https://doi.org/10.1088/1361-6463/aa63b4

Letter

# Tuning shape, composition and magnetization of 3D cobalt nanowires grown by focused electron beam induced deposition (FEBID)

**Javier Pablo-Navarro[1], Dédalo Sanz-Hernández[2], César Magén[1,3,4], Amalio Fernández-Pacheco[2] and José María de Teresa[1,3,5]**

[1] Laboratorio de Microscopías Avanzadas (LMA), Instituto de Nanociencia de Aragón (INA), Universidad de Zaragoza, 50018 Zaragoza, Spain
[2] Cavendish Laboratory, University of Cambridge, JJ Thomson Cambridge, CB3 0HE, United Kingdom
[3] Departamento de Física de la Materia Condensada, Universidad de Zaragoza, 50009 Zaragoza, Spain
[4] Fundación ARAID, Zaragoza, Spain
[5] Facultad de Ciencias, Instituto de Ciencia de Materiales de Aragón, Universidad de Zaragoza—CSIC, 50009 Zaragoza, Spain

E-mail: deteresa@unizar.es

Received 23 December 2016, revised 23 February 2017
Accepted for publication 1 March 2017
Published 3 April 2017

Invited by Andreas Berger

**Abstract**

Electron beam induced deposition of 3D cobalt nanowires with simultaneous high metallic content (≈80% at.) and small diameter (<100 nm) has been achieved by optimization of the growth parameters. Two different growth modes have been identified, denoted as *radial* and *linear*. In the *radial* mode, the wire diameter is at least ≈120 nm and the Co content is greater than ≈85% at. In the *linear* mode, the diameter is smaller than 80 nm and the Co content is at best ≈80% at. A sharp transition between both growth modes can occur inside a single nanowire for certain experimental conditions. Electron holography measurements indicate that in optimized Co nanowires the magnetic induction is high enough for applications in spintronics, magnetic sensing and actuation at the nanoscale.

Keywords: cobalt nanowires, focused electron beam induced deposition, electron holography, magnetic nanowires

(Some figures may appear in colour only in the online journal)



 

## 1. Introduction

Thin-film layers and multilayers based on magnetic materials have nowadays various applications in the fields of sensors and data storage, like in hard disks [1, 2]. On the other hand, individual magnetic nanostructures are being investigated for their potential application in sensors [3], memories [4] and logic [5]. Although most of the approaches for their fabrication rely on standard lithography processes performed onto magnetic thin films and multilayers, a growing interest exists on 3D magnetic nanostructures, whose fabrication is challenging. Focused electron beam induced deposition (FEBID) is one of the techniques that allow the growth of 3D structures to be addressed [6–10], in particular those based on magnetic materials [11–20]. In FEBID, precursor molecules delivered by a gas injection system (GIS) close to the substrate become dissociated by a focused electron beam, producing a deposit [21–24]. The shape of the deposit is determined by the electron beam scan as well as complex interactions between electron beam, substrate, precursor molecules and the growing structure [25, 26]. The use of precursor molecules containing magnetic elements such as Co, Fe and Ni permits the growth of magnetic deposits [11, 27–33] and a large development has been made towards the growth of magnetic deposits with high metal content, high magnetization, high resolution and complex shapes, as recently reviewed [34, 35]. Such development has been focused on the optimization of thin in-plane magnetic layers, whereas limited work has been done with regard to 3D magnetic deposits. However, there are many promising applications of 3D magnetic deposits in scanning probe techniques (such as magnetic force microscopy [17] and ferromagnetic resonance force microscopy [36]), racetrack-type magnetic memories [14], Hall sensors [37, 38], nano-magnet logic [17, 39], superconducting vortex lattice pinning [40], remote magneto-mechanical actuation [20], etc.

In the present work, we investigate in detail the interplay of the precursor flux and the electron beam current in the physical properties of out-of-plane magnetic nanowires grown by FEBID using the $Co_2(CO)_8$ precursor. Our focus is put on the characterization of the obtained nanowire's diameter, composition and magnetization, with the aim of growing narrow nanowires (<100 nm in diameter), with high Co content (>80% at.) and magnetization approaching the bulk value (1.8 T).

Previous work on the growth of 3D nanowires by FEBID has shown the relevance of several parameters that should be taken into account. For example, the use of sub-nA electron beam currents produced by field-emission guns is suitable for the growth of narrow nanowires (<100 nm in diameter) [14, 41]. Additionally, the interaction of the primary electron beam with the substrate and the growing structure also depends on the primary electron beam energy [42, 43]. The balance between the availability of precursor molecules on the growth area and the electron beam current is very important because it will determine whether the growth occurs in the precursor-limited regime or the electron-limited regime, which will affect not only the growth rate but also the composition of the nanowire [44]. However, this equilibrium can be strongly modified when thermal heating of the growing deposit occurs, as previously found in FEBID [45–48]. On the one hand, an increase of temperature in the area of growth will change the precursor residence time, affecting the growth rate and potentially the growth regime. On the other hand, the decomposition of the precursor molecules will be faster if temperatures close to the thermal decomposition of the precursor are reached. Moreover, thermal effects can be of tremendous importance in 3D nanostructures given that precursor replenishment in the area of growth occurs at a lower rate compared to in-plane deposits because the diffusion mechanism of precursor molecules from the substrate will be weakened as the deposit grows in height. In fact, our results presented hereafter have identified a set of growth parameters that produce a change in the diameter during the growth of a single nanowire. This is a consequence of the subtle balance between the different factors governing the growth of 3D nanowires, as discussed hereafter.

## 2. Experimental

### 2.1. Growth of the 3D nanowires by FEBID

The nanowires were grown in commercial Helios Nanolab 600 and 650 Dual Beam equipment using a Schottky field-emission electron gun (S-FEG) and a GIS that delivers the $Co_2(CO)_8$ precursor. The substrates were TEM copper grids. FEBID-Co deposits were grown with low electron beam currents (<100 pA). The working voltage was fixed to 5 kV, given that initial experiments did not lead to significant changes in the composition from 5 kV to 30 kV. The nanowires were grown in spot mode, where the electron beam is continuously irradiating a single point. A base pressure of $1 \times 10^{-6}$ mbar existed in the working chamber before the injection of the precursor. The $Co_2(CO)_8$ precursor flux was tuned via a manual valve, which permits us to vary the chamber pressure during growth up to ~$4 \times 10^{-5}$ mbar. Given the linear relationship between the chamber pressure increase during gas injection ($\Delta P$) and the precursor flux ($J$), $J \alpha \Delta P$ [49], monitorization of the chamber pressure during growth allows us to establish correlations between them.

### 2.2. Compositional analysis by energy dispersive x-ray spectroscopy

Some of the energy dispersive x-ray spectroscopy (EDS) experiments were performed in the Helios Nanolab 650 Dual Beam equipment, using an electron beam voltage of 5 kV and a beam current of 800 pA, analyzed with EDAX software using the APOLLO X detector. Other EDS experiments were carried out inside an FEI Tecnai F30 transmission electron microscopy (TEM) equipment operated at 300 kV. In this case, an EDAX 136-5 detector was used with the Genesis RTEM software embedded in FEI's TIA software. The material composition was determined through these experiments with a typical error of ~2% at. for main components assuming uniform composition in the nanostructure. Within the manuscript, the composition is always expressed in at.%.

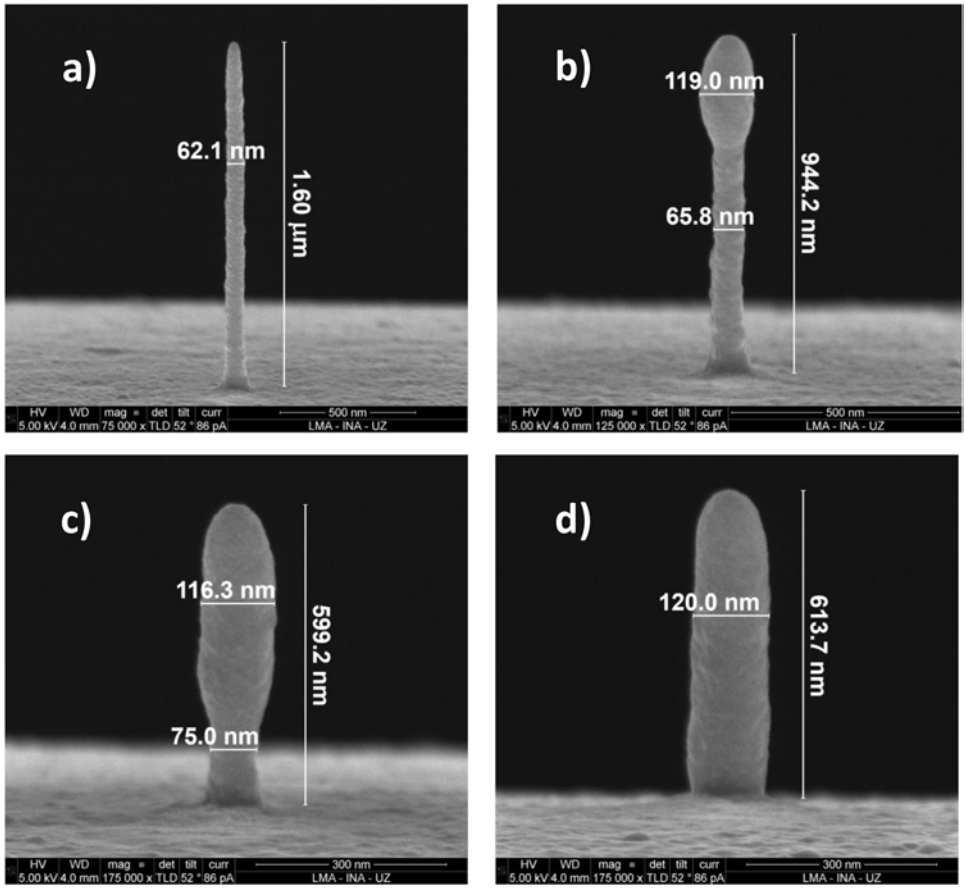


**Figure 1.** SEM images of cobalt nanowires grown under the following conditions: electron beam voltage of 5 kV, beam current of 86 pA and working pressure (minus base pressure) of (a) $7.3 \times 10^{-6}$ mbar, (b) $6.4 \times 10^{-6}$ mbar, (c) $5.9 \times 10^{-6}$ mbar, and (d) $5.1 \times 10^{-6}$ mbar. The transition from linear to radial growth mode with decreasing precursor flux is noticed.

### *2.3. Compositional analysis by energy electron loss spectroscopy*

Energy electron loss spectroscopy (EELS) experiments were performed in an FEI Tecnai F30 equipment and in probe-corrected Titan Low Base 60–300 equipment, both operated at 300 kV. The first one is fitted with an S-FEG and a Tridiem 863 Gatan energy filter (GIF), whereas the second one is equipped with a high brightness S-FEG, a CETCOR corrector for the condenser system to provide sub-Angstrom probe size, and a Tridiem GIF 866 ERS. The spectroscopic experiments were carried out with a 25 mrad convergence semi-angle and EELS spectra were performed with an energy dispersion of 0.8 eV and energy resolution around 1.5 eV.

### *2.4. Analysis of the magnetic induction by electron holography inside a transmission electron microscope*

Electron holography (EH) was carried out in image-corrected FEI Titan Cube 60–300 TEM equipment operated at 300 kV, equipped with an S-FEG and a CETCOR corrector for the objective lens and a motorized electrostatic biprism. The experiments were performed in Lorentz mode (with the objective lens switched off, and the Lorentz lens, fitted below the objective lens, operating as the image-forming lens). In the holographic experiments, the excitation of the biprism was varied between 180 V and 220 V, depending on the actual diameter of the nanowires, to produce holograms with a fringe contrast range of 20–25%. The acquisition time of the holograms was set to 5 s. The method to extract the magnetic induction has been described in detail in a previous publication [41].

## 3. Results

As previously mentioned, a low electron beam current is a pre-requisite for the growth of small-diameter nanowires. First, we present the results obtained using an electron beam current of 86 pA. As can be observed in figure 1(a), a narrow nanowire with a diameter of 62 nm and an aspect ratio of 25 is obtained when $\Delta P$ is $7.3 \times 10^{-6}$ mbar. However, a decrease in $\Delta P$ to $6.4 \times 10^{-6}$ mbar provokes a change in the growth mode at the height of 650 nm, resulting in a nanowire with a small diameter in the first segment (66 nm) and a larger diameter in the second one (119 nm), as shown in figure 1(b). A further decrease in $\Delta P$ to $5.9 \times 10^{-6}$ mbar induces the appearance of the larger diameter closer to the substrate, at the height of 160 nm (see figure 1(c)). If an even lower $\Delta P$ of $5.1 \times 10^{-6}$ mbar is used, the nanowire grows from the beginning in the mode with a larger diameter, 120 nm, as shown in figure 1(d). Hereafter, the growth mode with the smaller diameter is referred to as the 'linear regime' whereas the growth

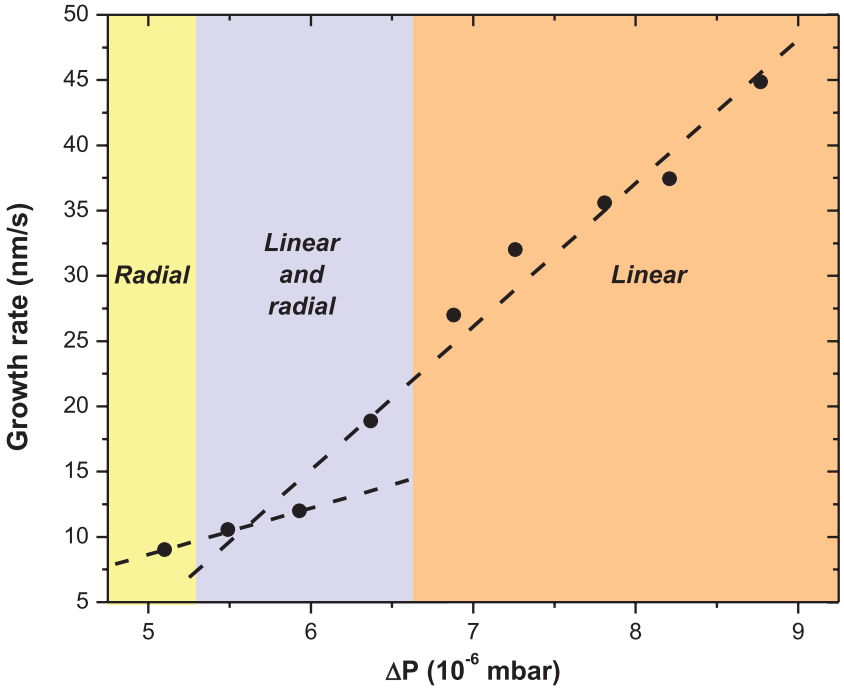


**Figure 2.** Growth rate of nanowires grown at an electron beam voltage of 5 kV and a beam current of 86 pA as a function of the working pressure (minus base pressure). A change in slope is noticed at the crossover from radial to linear growth modes. In the 'linear and radial' growth mode, the nanowire presents two segments, one with the features of the linear mode and one with the features of the radial mode.

mode with the larger diameter is referred to as the 'radial regime'. It is experimentally observed that if the growth current is increased, the radial-to-linear crossover occurs at higher precursor flux (chamber growth pressure). A quantitative model to explain this change in the mode of growth is beyond the scope of the present article given its complexity, but is being currently addressed by the authors. Thermal and/or diffusion effects are expected to play a crucial role in the observed effect. Thus, an increased thermal desorption of the precursor [50] will occur due to an increased temperature at the tip of the nanowire due to reduced thermal dissipation at long wire lengths. Additionally, a reduced number of molecules will be able to diffuse from the substrate as the nanowire grows.

Similarly to the case of in-plane deposits, the height growth rate of the obtained nanowires increases with the working pressure, as shown in figure 2, and is indicative of growth in the precursor-limited regime [44]. However, as noticed in this figure, a change in the growth rate slope is observed at the crossover between the linear and radial growth modes, highlighted with two visual guide lines. It should be stressed that the average height growth rate is well defined for nanowires with pure linear or radial growth modes but, in the case of nanowires with transition between both modes, this value will depend on the relative contribution of both segments to the total height. The height growth rate was determined from data in table 1 considering the total height of the nanowire and the deposition time, defined as the time spent to grow it. Additionally, the volume growth rate as a function of the working pressure was calculated, increasing linearly in the linear growth mode.

As shown in figure 3, the composition of the deposits is strongly affected by the precursor flux. A dedicated

**Table 1.** Data of the nanowires represented in figure 2: height, deposition time, growth rate and working pressure (minus base pressure) during growth.

| Height ($\mu$m) | Deposition time (s) | Growth rate (nm $s^{-1}$) | $\Delta P$ ($10^{-6}$ mbar) |
|---|---|---|---|
| 1.66 | 37 | 44.9 | 8.8 |
| 1.61 | 43 | 37.4 | 8.2 |
| 1.53 | 43 | 35.6 | 7.8 |
| 1.60 | 50 | 32.0 | 7.3 |
| 1.35 | 50 | 27.0 | 6.9 |
| 0.944 | 50 | 18.9 | 6.4 |
| 0.599 | 50 | 12.0 | 5.9 |
| 0.655 | 62 | 10.6 | 5.5 |
| 0.614 | 68 | 9.0 | 5.1 |

experiment was performed in which the electron beam current was fixed to 100 pA. At that beam current, the crossover from the radial-growth regime to the linear-growth regime occurs at $\Delta P$ of $1.75 \times 10^{-5}$ mbar. Overall, the behavior of the Co content as a function of working pressure resembles that observed in in-plane deposits [38]: an optimum precursor flux window ($1 \times 10^{-5}$ mbar $< \Delta P < 1.5 \times 10^{-5}$ mbar) exists where the Co content is high (~85%). Although specific experiments and/or simulations could shed more light on the origin of this change in composition, from general arguments it can be stated that at lower precursor flux the Co content can diminish due to decomposition of residual contaminant species in the chamber, whereas at higher precursor flux the Co content can diminish due to incomplete precursor decomposition. The different origin of the decreased Co content at low and high precursor flux can be also noted in the C/O ratio, which is smaller than 1 at high precursor flux and larger than

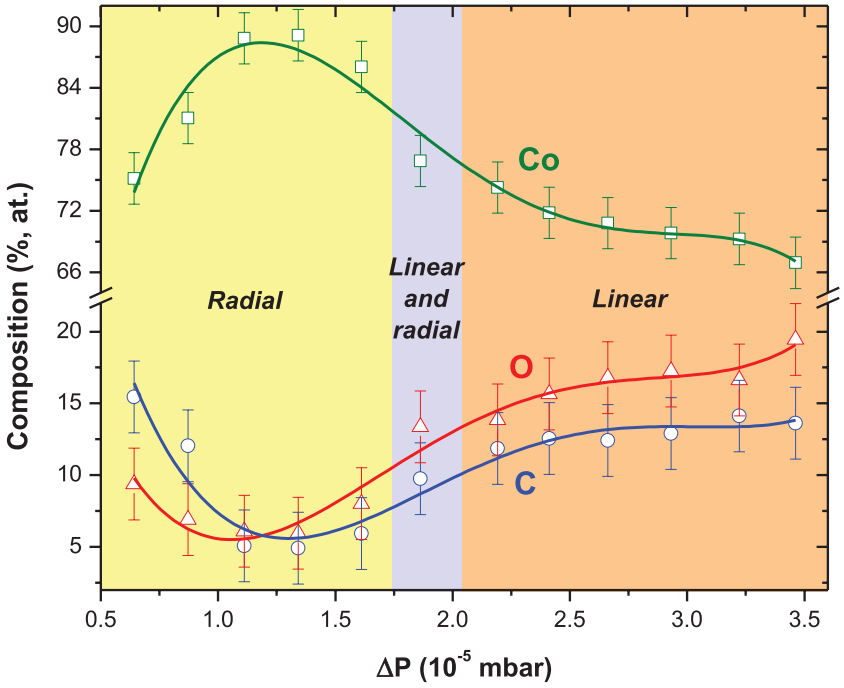


**Figure 3.** Composition of nanowires grown using an electron beam voltage of 5 kV and a beam current of 100 pA as a function of the working pressure (minus base pressure). EDS measurements were performed at 5 kV and 800 pA. Three different growth regimes can be noticed. The composition of the sample falling in the 'linear and radial' regime has been determined at the base of the nanowire, which corresponds to the linear-growth mode.

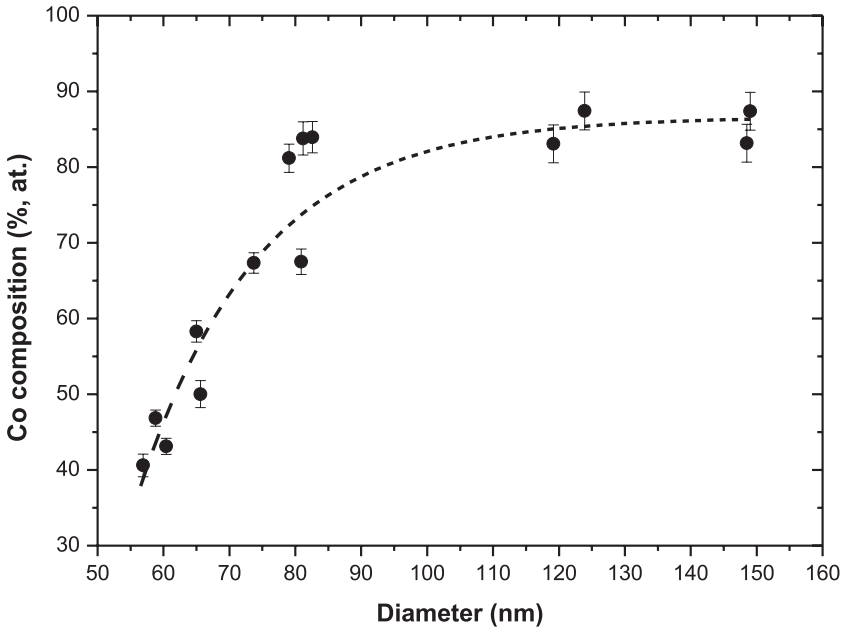


**Figure 4.** Cobalt composition as a function of the wire diameter for optimized growth conditions at each particular value of the diameter.

1 at low precursor flux (see figure 3). From figure 3, it is clear that optimum Co content (>85%) can be only achieved in the radial-growth mode, where the diameter is at least ≈120 nm.

In order to correlate the Co content of the nanowires with their magnetization, dedicated experiments have been carried out inside the TEM. The experiment consists of EDS of all nanowires and EELS of two selected nanowires. EH has also been performed on selected individual nanowires to obtain quantitative values of the Co content and the magnetic induction inside the nanowire. In figure 4, the Co content is represented as a function of the nanowire's diameter for optimum growth conditions. The specific growth parameters of each nanowire displayed in figure 4 are described in table 2. Figure 4 indicates that a high Co content (>85%) can be achieved in nanowires with a diameter larger than ≈120 nm, which correspond to the radial-growth mode. However, the Co content in nanowires with a diameter smaller than ≈80 nm, which correspond to the linear-growth mode, is around 80% for diameters of ≈80 nm, but diminishes quickly as the diameter is reduced. For diameters of ≈60 nm, the Co content is

**Table 2.** Data of the nanowires represented in figure 4: diameter, Co content and technique used for its measurement, beam current and working pressure (minus base pressure) during growth. The beam energy used for the growth was 5 kV.

| Diameter (nm) | Co composition (%, at.) | Technique | Growth current (pA) | $\Delta P$ ($10^{-6}$ mbar) |
|---|---|---|---|---|
| 56.9 | 40.6 | EDS | 50 | 2.8 |
| 58.8 | 46.9 | EDS | 25 | 10.3 |
| 60.4 | 43.1 | EDS | 50 | 10.2 |
| 65.0 | 58.3 | EDS | 100 | 10.5 |
| 65.6 | 50.0 | EDS | 100 | 9.3 |
| 73.7 | 67.3 | EDS | 100 | 8.1 |
| 79.1 | 81.2 | EDS | 50 | 6.9 |
| 80.9 | 67.5 | EDS | 100 | 8.1 |
| 81.2 | 83.8 | EDS | 100 | 8.4 |
| 82.6 | 84.0 | EDS | 50 | 7.8 |
| 119.2 | 83.1 | EELS | 50 | 2.8 |
| 123.9 | 87.4 | EDS | 50 | 5.2 |
| 148.5 | 83.2 | EDS | 100 | 6.9 |
| 149.0 | 87.4 | EELS | 100 | 6.1 |

only ~45%. Given that the nanowires present typical oxidized shells of around 5 nm [41], the measured average Co content will be lower as the wire diameter decreases. This means that in the core of the nanowire the Co content is expected to be higher than the average value, this effect being more significant for the narrowest wires.

The magnetic induction of selected nanowires has been investigated by means of EH. Each nanowire is measured in magnetic remanence after previously saturating the magnetization in two opposite directions by applying an external magnetic field produced by the objective lens. This is a common method to get rid of the electrostatic contribution to the phase change and to reveal the magnetic contribution after subtraction of both measurements. Following the EH method described in a previous work [41], the average magnetic induction inside a nanowire along its long axis, $B_x$, can be calculated as:

$$|B_x(x,y)| = \frac{\hbar}{e \cdot t} \frac{\partial \varphi_{\mathrm{MAG}}(x,y)}{\partial y} \quad (1)$$

where $\hbar$ is the reduced Planck constant, $\varphi_{\mathrm{MAG}}$ is the magnetic component of the total electron phase shift $\varphi(\vec{r})$, $e$ is the electron charge and $t$ is the variable thickness along the specimen width. In figure 5, the results corresponding to three nanowires, representative of the three regimes found in this study, are shown. The values obtained for $B_x$ close to the nanowire borders are not reliable due to the uncertainties in the sample thickness at those positions and edge effects at the oxidized wire surface. For this reason, in figure 5 the values of $B_x$ obtained at the edges of the nanowires are masked with a semi-transparent band. However, the values obtained in the central part of the nanowires are trustworthy. The nanowire with the largest diameter, 123.9 nm, corresponding to the radial-growth mode, presents a high magnetic induction along the long wire axis of ~1.33 T, not far from the bulk value, 1.8 T. This high value of the magnetization correlates well with the high Co content in the nanowire, 87.4%. A second nanowire, corresponding to the intermediate linear-radial-growth mode has been analyzed by EH at the base, in the portion with linear-growth mode. It presents a magnetic induction along the long wire axis of 0.78 T, around 50% of the bulk magnetization of Co. This reduction is expected given the reduced Co content (67.5%) in this nanowire. A third nanowire, corresponding to the linear-growth mode, presents a lower magnetic induction along the long wire axis of 0.41 T, which can be expected given its reduced Co content (40.6%). However, we would like to point out that the obtained magnetic induction in the nanowires is sufficiently high for functional nanomagnetic devices and applications. Just as an example, the Fe magnetic rods used in the past by Franken *et al* had magnetization of 0.13 T along their long axis and were able to pin domain walls in a domain-wall conduit [16].

## 4. Discussion

FEBID growth of functional magnetic nanostructures requires precise control of a high number of growth parameters. Their precise tuning can be crucial in particular cases, such as the growth of 3D Co nanowires discussed in the present work. In the process of optimization of their growth, we have encountered a number of interesting phenomena that should be taken into account for their practical application. The first important finding regards the existence of two growth modes with different physical properties, denoted as linear and radial due to certain similarities with the reported growth of 3D iron nanowires [45]. In the radial-growth mode, the minimum diameter obtained is ≈120 nm and the Co content can be very high, >85%, showing a high magnetization, not far from the bulk value, 1.8 T. In the linear-growth mode, the diameter can be lower than ≈80 nm and the Co content diminishes for the decreasing diameter. For a diameter of 80 nm, nanowires can attain Co content of 80% and show magnetization around half the bulk value. However, if the diameter is 60 nm, the Co content is found to be 45% and the magnetization is around 1/4 of the bulk value. We cannot discard that the nanowires of low Co content have areas with inhomogeneous composition, the areas richer in Co contributing more to the magnetization of the nanowire. Interestingly, inside the same nanowire, a transition between both growth modes can be observed in a certain range of growth parameters. This effect seems to indicate that thermal desorption and decreased diffusion effects during the growth of high-aspect-ratio 3D nanostructures may be playing a key role. The capacity to dissipate the heat caused by the electron beam is reduced as the nanowire grows and the tip grows progressively further away from the substrate. At a certain height, there is an overheating which could result in a change of the growth mode. The existence of single nanowires with two diameters seems useful for studies of magnetic-domain-wall propagation in nanowires, given their tendency to become pinned at the location of the transition between both diameters [51].

The correlation found between the diameter of the nanowire and its composition is important given the relationship

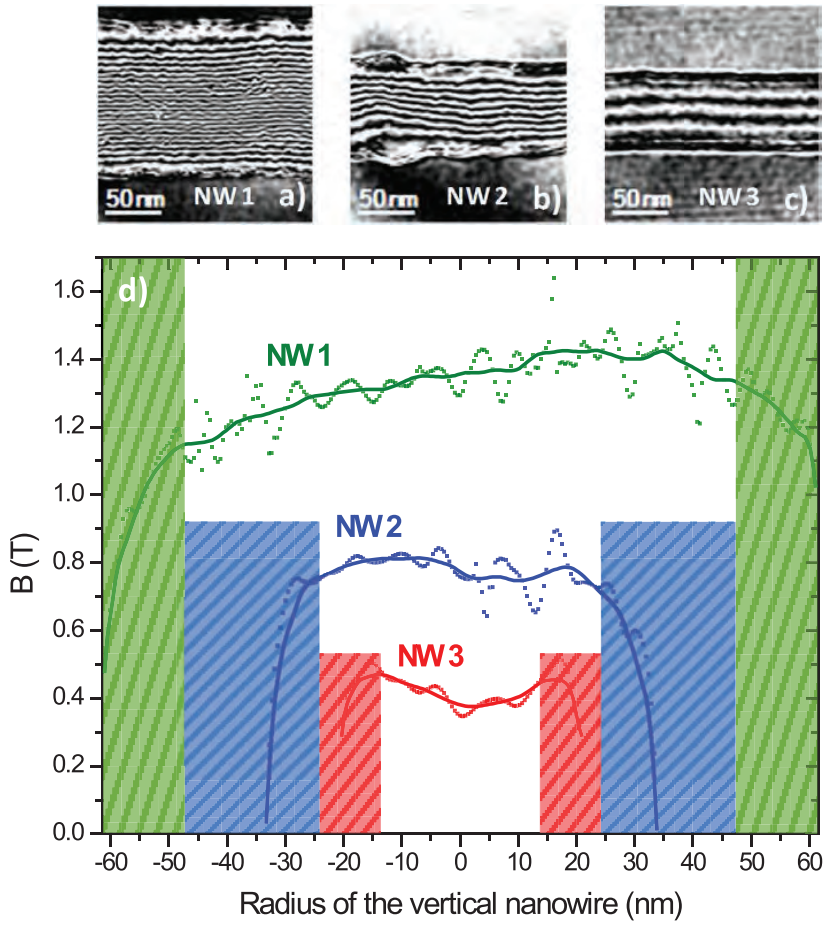


**Figure 5.** (a) Representation of the magnetic induction flux of a nanowire with the cobalt content of 87.4% at. (NW1), obtained from the magnetic phase images after normalizing by the maximum thickness and performing the cosine of 700 times the change in the normalized electron phase; (b) the same for the nanowire with the cobalt content of 67.5% at. (NW2); (c) the same for the nanowire with the cobalt content of 40.6% at. (NW3); (d) profiles of the magnetic induction along the short axis of nanowires NW1, NW2 and NW3, obtained from the magnetic phase images used to calculate (a)–(c), respectively. The edges of the nanowires are partially masked given that quantification is not reliable due to edge effects.

observed between the Co content and the magnetization of the nanowire. If a nanowire with magnetization close to the bulk value, 1.8 T, is required, the best option is to grow a nanowire with diameter of at least 120 nm. However, in many practical situations, narrow nanowires (<100 nm) are required, in which case, a maximum Co content of ~80% can be achieved, this value diminishing strongly with decreasing diameter. In such a situation, the magnetization is observed to decrease with respect to the bulk value despite being still quite large in absolute value. There are a few potential applications of these nanowires, such as magnetic functionalization of cantilevers [11, 13, 17, 52, 53], 3D logic structures [17, 39], cylindrical conduits for domain-wall propagation [14], superconducting vortex lattice pinning [40, 54], remote magnetomechanical actuation [20], etc, where lateral resolution is more important than the absolute value of the magnetization. In those cases, the type of nanowire grown here in the linear-growth mode meets the required physical properties. Another strategy to enhance the Co content is to perform post-annealing treatments [55, 56]. It has been shown that in-plane Co structures can be purified by annealing in vacuum conditions, eliminating the oxygen content of the deposits [56]. This could be a viable strategy to obtain narrow Co nanowires (<100 nm in diameter) with very high Co content (>90%) and the associated magnetization close to the bulk value.

## 5. Conclusions

To conclude, we have shown that control of the growth parameters in focused electron beam induced deposition, especially the electron beam current and the precursor flux, allows the tuning of the diameter, composition and magnetization of 3D cobalt nanowires, grown using the $Co_2(CO)_8$ precursor. A transition between two growth modes, radial and linear, has been unveiled in single nanowires, resulting in individual nanowires with two different diameters (80 nm and 120 nm, respectively). The best growth conditions to achieve nanowires with a small diameter (<80 nm), high metallic content (~80%) and high magnetization (~0.9 T) have been identified, providing a growth route for various applications.

## Acknowledgment

This work was supported by the Spanish Ministry of Economy and Competitivity through projects No. MAT2014-51982C2-1-R, MAT2014-51982C2-2-R and MAT2015-69725-REDT, including FEDER funds and by the Aragon Regional Government (Construyendo Europa desde Aragón) through project E26, with FEDER funding. This work was conducted within the framework of the COST Action CM1301 (CELINA). AFP acknowledges funding from a EPSRC Early Career Fellowship EP/M008517/1 and from a Winton Fellowship. In order to comply with EPSRC policy on research data, all metadata associated to this publication can be accessed via https://doi.org/10.17863/CAM.8106. JP-N grant is funded by the *Ayuda para Contratos Predoctorales para la Formación de Doctores, Convocatoria Res.* 05/06/15 (BOE 12/06/15) of the *Secretaría de Estado de Investigación, Desarrollo e Innovación* in the *Subprograma Estatal de Formación* of the Spanish Ministry of Economy and Competitiveness (MINECO) with the participation of the European Social Fund. Experimental help clean-room technicians from 'Laboratorio de Microscopías Avanzadas' (LMA) are warmly acknowledged. Discussions with Dr Luis Serrano-Ramón about the growth conditions and the nature of the linear and radial growth modes are acknowledged.

## References

[1] Hartmann U 2000 *Magnetic Multilayers and Giant Magnetoresistance: Fundamentals and Industrial Applications* (Berlin: Springer)
[2] Fert A 2008 Origin, development, and future of spintronics (Nobel lecture) *Rev. Mod. Phys.* **80** 1517–30
[3] Candini A, Gazzadi G C, Di Bona A, Affronte M, Ercolani D, Biasiol G and Sorba L 2006 Hall nano-probes fabricated by focused ion beam *Nanotechnology* **17** 2105–9
[4] Chappert C, Fert A and Van Dau F N 2007 The emergence of spin electronics in data storage *Nat. Mater.* **6** 813–23
[5] Niemier M T *et al* 2011 Nanomagnet logic: progress toward system-level integration *J. Phys.: Condens. Matter* **23** 493202
[6] Castagné M, Benfedda M, Lahimer S, Falgayrettes P and Fillard J P 1999 Near field optical behaviour of C supertips *Ultramicroscopy* **76** 187–94
[7] Gazzadi G C, Frabboni S and Menozzi C 2007 Suspended nanostructures grown by electron beam-induced deposition of Pt and TEOS precursors *Nanotechnology* **18** 445709
[8] Bøggild P, Hansen T M, Tanasa C and Grey F 2001 Fabrication and actuation of customized nanotweezers with a 25 nm gap *Nanotechnology* **12** 331–5
[9] Höflich K, Yang R B, Berger A, Leuchs G and Christiansen S 2011 The direct writing of plasmonic gold nanostructures by electron-beam-induced deposition *Adv. Mater.* **23** 2657–61
[10] Fowlkes J D, Winkler R, Lewis B B, Stanford M G, Plank H and Rack P D 2016 Simulation-Guided 3D nanomanufacturing via focused electron beam induced deposition *ACS Nano* **10** 6163–72
[11] Utke I, Hoffmann P, Berger R and Scandella L 2002 High-resolution magnetic Co supertips grown by a focused electron beam *Appl. Phys. Lett.* **80** 4792–4
[12] Takeguchi M, Shimojo M, Che R and Furuya K 2006 Fabrication of a nano-magnet on a piezo-driven tip in a TEM sample holder *J. Mater. Sci.* **41** 2627–30
[13] Belova L M, Hellwig O, Dobisz E and Dan Dahlberg E 2012 Rapid preparation of electron beam induced deposition Co magnetic force microscopy tips with 10 nm spatial resolution *Rev. Sci. Instrum.* **83** 093711
[14] Fernández-Pacheco A, Serrano-Ramón L, Michalik J M, Ibarra M R, de Teresa J M, O'Brien L, Petit D, Lee J and Cowburn R P 2013 Three dimensional magnetic nanowires grown by focused electron-beam induced deposition *Sci. Rep.* **3** 1492
[15] Lavenant H 2014 Mechanical magnetometry of Cobalt nanospheres deposited by focused electron beam at the tip of ultra-soft cantilevers *Nanofabrication* **1** 65–73
[16] Franken J H, Van Der Heijden M A J, Ellis T H, Lavrijsen R, Daniels C, McGrouther D, Swagten H J M and Koopmans B 2014 Beam-induced Fe nanopillars as tunable domain-wall pinning sites *Adv. Funct. Mater.* **24** 3508–14
[17] Gavagnin M, Wanzenboeck H D, Wachter S, Shawrav M M, Persson A, Gunnarsson K, Svedlindh P, Stöger-Pollach M and Bertagnolli E 2014 Free-standing magnetic nanopillars for 3D nanomagnet logic *ACS Appl. Mater. Interfaces* **6** 20254–60
[18] Gazzadi G C and Frabboni S 2015 Structural transitions in electron beam deposited Co-carbonyl suspended nanowires at high electrical current densities *Beilstein J. Nanotechnol.* **6** 1298–305
[19] Perez-Roldan M J, Tatti F, Vavassori P, Berger A and Chuvilin A 2015 Segregation of materials in double precursor electron-beam-induced-deposition: a route to functional magnetic nanostructures *Nanotechnology* **26** 375302
[20] Vavassori P, Pancaldi M, Perez-Roldan M J, Chuvilin A and Berger A 2016 Remote magnetomechanical nanoactuation *Small* **12** 1013–23
[21] Randolph S J, Fowlkes J D and Rack P D 2006 Focused, nanoscale electron-beam-induced deposition and etching *Crit. Rev. Solid State Mater. Sci.* **31** 55–89
[22] Van Dorp W F and Hagen C W 2008 A critical literature review of focused electron beam induced deposition *J. Appl. Phys.* **104** 81301
[23] Utke I, Hoffmann P and Melngailis J 2008 Gas-assisted focused electron beam and ion beam processing and fabrication *J. Vac. Sci. Technol.* B **26** 1197–276
[24] Huth M, Porrati F, Schwalb C, Winhold M, Sachser R, Dukic M, Adams J and Fantner G 2012 Focused electron beam induced deposition: a perspective *Beilstein J. Nanotechnol.* **3** 597–619
[25] Plank H, Smith D A, Haber T, Rack P D and Hofer F 2012 Fundamental proximity effects in focused electron beam induced deposition *ACS Nano* **6** 286–94
[26] Winkler R, Szkudlarek A, Fowlkes J D, Rack P D, Utke I and Plank H 2015 Toward ultraflat surface morphologies during focused electron beam induced nanosynthesis: disruption origins and compensation *ACS Appl. Mater. Interfaces* **7** 3289–97
[27] Fernández-Pacheco A, de Teresa J M, Córdoba R and Ibarra M R 2009 Magnetotransport properties of high-quality cobalt nanowires grown by focused-electron-beam-induced deposition *J. Phys. D: Appl. Phys.* **42** 55005
[28] Takeguchi M, Shimojo M and Furuya K 2005 Fabrication of magnetic nanostructures using electron beam induced chemical vapour deposition *Nanotechnology* **16** 1321–5
[29] Lavrijsen R *et al* 2011 Fe:O:C grown by focused-electron-beam-induced deposition: magnetic and electric properties *Nanotechnology* **22** 25302

[30] Perentes A, Sinicco G, Boero G, Dwir B and Hoffmann P 2007 Focused electron beam induced deposition of nickel *J. Vac. Sci. Technol.* B **25** 2228
[31] Córdoba R, Barcones B, Roelfsema E, Verheijen M A, Mulders J J L, Trompenaars P H F and Koopmans B 2016 Functional nickel-based deposits synthesized by focused beam induced processing *Nanotechnology* **27** 65303
[32] Nikulina E, Idigoras O, Porro J M, Vavassori P, Chuvilin A and Berger A 2013 Origin and control of magnetic exchange coupling in between focused electron beam deposited cobalt nanostructures *Appl. Phys. Lett.* **103** 123112
[33] Gavagnin M, Wanzenboeck H D, Belic D, Shawrav M M, Persson A, Gunnarsson K, Svedlindh P and Bertagnolli E 2014 Magnetic force microscopy study of shape engineered FEBID iron nanostructures *Phys. Status Solidi* a **211** 368–74
[34] de Teresa J M and Fernández-Pacheco A 2014 Present and future applications of magnetic nanostructures grown by FEBID *Appl. Phys.* A **117** 1645–58
[35] de Teresa J M, Fernández-Pacheco A, Córdoba R, Serrano-Ramón L, Sangiao S and Ibarra M R 2016 Review of magnetic nanostructures grown by focused electron beam induced deposition (FEBID) *J. Phys. D: Appl. Phys.* **49** 243003
[36] Guo F, Belova L M and McMichael R D 2013 Spectroscopy and imaging of edge modes in permalloy nanodisks *Phys. Rev. Lett.* **110** 017601
[37] Gabureac M, Bernau L, Utke I and Boero G 2010 Granular Co–C nano-Hall sensors by focused-beam-induced deposition *Nanotechnology* **21** 115503
[38] Serrano-Ramón L, Córdoba R, Rodríguez L A, Magén C, Snoeck E, Gatel C, Serrano I, Ibarra M R and de Teresa J M 2011 Ultrasmall functional ferromagnetic nanostructures grown by focused electron-beam-induced deposition *ACS Nano* **5** 7781–7
[39] Sharma N, van Mourik R A, Yin Y, Koopmans B and Parkin S S P 2016 Focused-electron-beam-induced-deposited cobalt nanopillars for nanomagnetic logic *Nanotechnology* **27** 165301
[40] Dobrovolskiy O V, Begun E, Huth M, Shklovskij V A and Tsindlekht M I 2011 Vortex lattice matching effects in a washboard pinning potential induced by Co nanostripe arrays *Physica* C **471** 449–52
[41] Pablo-Navarro J, Magén C and de Teresa J M 2016 Three-dimensional core–shell ferromagnetic nanowires grown by focused electron beam induced deposition *Nanotechnology* **27** 285302
[42] Belić D, Shawrav M M, Gavagnin M, Stöger-Pollach M, Wanzenboeck H D and Bertagnolli E 2015 Direct-write deposition and focused-electron-beam-induced purification of gold nanostructures *ACS Appl. Mater. Interfaces* **7** 2467–79
[43] Córdoba R, Sharma N, Kölling S, Koenraad P M and Koopmans B 2016 High-purity 3D nano-objects grown by focused-electron-beam induced deposition *Nanotechnology* **27** 355301
[44] Wachter S, Gavagnin M, Wanzenboeck H D, Shawrav M M, Belić D and Bertagnolli E 2014 Nitrogen as a carrier gas for regime control in focused electron beam induced deposition *Nanofabrication* **1** 16–22
[45] Hochleitner G, Wanzenboeck H D and Bertagnolli E 2008 Electron beam induced deposition of iron nanostructures *J. Vac. Sci. Technol.* B **26** 939
[46] Córdoba R, Sesé J, de Teresa J M and Ibarra M R 2010 High-purity cobalt nanostructures grown by focused-electron-beam-induced deposition at low current *Microelectron. Eng.* **87** 1550–3
[47] Belova L M, Dahlberg E D, Riazanova A, Mulders J J L, Christophersen C and Eckert J 2011 Rapid electron beam assisted patterning of pure cobalt at elevated temperatures via seeded growth *Nanotechnology* **22** 145305
[48] Van Dorp W F, Hansen T W, Wagner J B and De Hosson J T M 2013 The role of electron-stimulated desorption in focused electron beam induced deposition *Beilstein J. Nanotechnol.* **4** 474–80
[49] Serrano-Esparza I, Córdoba R, Mulders J J L, Ibarra M R and de Teresa J M 2015 Precursor competition in focused-ion-beam-induced co-deposition from $W(CO)_6$ and $C_{10}H_8$ *Sci. Lett. J.* **4** 127
[50] Szkudlarek A, Gabureac M and Utke I 2011 Determination of the surface diffusion coefficient and the residence time of adsorbates via local focused electron beam induced chemical vapour deposition *J. Nanosci. Nanotechnol.* **11** 8074–8
[51] Berganza E, Bran C, Jaafar M, Vázquez M and Asenjo A 2016 Domain wall pinning in FeCoCu bamboo-like nanowires *Sci. Rep.* **6** 29702
[52] Lau Y M, Chee P C, Thong J T L and Ng V 2002 Properties and applications of cobalt-based material produced by electron-beam-induced deposition *J. Vac. Sci. Technol.* A **20** 1295
[53] Tosolini G, Michalik J M, Córdoba R, de Teresa J M, Pérez-Murano F and Bausells J 2014 Magnetic properties of cobalt microwires measured by piezoresistive cantilever magnetometry *Nanofabrication* **1** 80–5
[54] Dobrovolskiy O V, Huth M and Shklovskij V A 2010 Anisotropic magnetoresistive response in thin Nb films decorated by an array of Co stripes *Supercond. Sci. Technol.* **23** 125014
[55] Begun E, Dobrovolskiy O V, Kompaniiets M, Sachser R, Gspan C, Plank H and Huth M 2015 Post-growth purification of Co nanostructures prepared by focused electron beam induced deposition *Nanotechnology* **26** 75301
[56] Puydinger dos Santos M V *et al* 2016 Annealing-based electrical tuning of cobalt–carbon deposits grown by focused-electron-beam-induced deposition *ACS Appl. Mater. Interfaces* **8** 32496–503